Journal of
Materials Chemistry A

Materials for energy and sustainability

rsc.li/materials-a

Volume 6
Number 12
28 March 2018
Pages 4883-5230

ISSN 2050-7488

**ROYAL SOCIETY
OF CHEMISTRY**

COMMUNICATION
Zhenhai Wen *et al.*
An electrochemically neutralized energy-assisted low-cost
acid-alkaline electrolyzer for energy-saving electrolysis
hydrogen generation

**ROYAL SOCIETY
OF CHEMISTRY**

rsc.li/materials-a

ARTICLE

Hydrogels with Highly Concentrated Salt Solution as Electrolytes for Solid-State Supercapacitors with Suppressed Self-Discharge Rate

Mingwei Shi,[a,b] Wei Yang,[a,b] Zailei Zhang,[a,b] Man Zhao,[a,b] Zhong Lin Wang,[a,b,c,*] and Xianmao Lu[a,b,*]

Solid-state supercapacitors (SSSCs) using hydrogel electrolytes have attracted great interest in recent years due to their potential for powering flexible and wearable electronics. But the application of SSSCs has been severely restricted by self-discharge, which is an inevitable issue that causes fast decay of cell voltage and loss of stored energy. In this work, we demonstrate that suppressed self-discharge of SSSCs can be achieved by using polyacrylamide (PAAm) hydrogel containing highly concentrated LiCl as electrolytes. Specifically, for cells with 14 M LiCl-PAAm hydrogel electrolyte charged to 0.8 V, a low OCV decay rate of 6.7×10^{-5} V mF^{-1} hr^{-1} and a small leakage current of 0.003 μA mF^{-1} V^{-1} are obtained. Notably, the leakage current is much smaller than currently reported supercapacitors using hydrogel electrolytes. In addition, when the SSSCs are employed for storing energy harvested by triboelectric nanogenerator (TENG) that has a characteristic of pulsed output current at μA scale, much enhanced charging efficiency is attained.

Introduction

With the growing demand of power for wearable and flexible electronic devices, solid-state energy storage devices have attracted great interest.[1] Particularly, significant efforts have been made on the development of solid-state supercapacitors (SSSCs) with hydrogel electrolytes. Such SSSCs (or quasi-solid-state supercapacitors) have shown improved energy densities and additional functions such as self-healing capability, shape memory, and stretchability.[1] However, much less attention has been paid on the self-discharge of SSSCs,[2-4] even though fast self-discharge has seriously limited their applications in energy storage, especially for devices used for 'standby' purposes.[5-8]

Typical SSSCs with hydrogel electrolytes have exhibited fast self-discharge, leading to rapid decay of open-circuit voltages (OCVs) to one-half of their charging voltages mostly within a few hours[9-12] or even just tens of minutes.[13] To address this issue, various approaches have been attempted in recent years.[3,4,14] For instance, carbon nanotubes as gel electrolyte additives have been used by Fan at al. to prevent the diffusion of redox species and reduce the self-discharge for SCs with redox-active ionic liquid-based gel polymer electrolytes.[14] A zwitterionic gel electrolyte based on poly(propylsulfonate dimethylammonium propylmethacrylamide) has also been employed to suppress the self-discharge of SCs.[3] In this gel electrolyte, the diffusion- and

activation-controlled faradaic reactions can be reduced due to the electrostatic attractions between the charged species and the zwitterionic groups so slow self-discharge rate has been achieved. Wang et al. introduced sodium polystyrene sulfonate (NaPSS) and poly (diallyl dimethylammonium chloride) (PDDACl) into polyvinyl alcohol (PVA) matrix gels to construct heterogeneous polymer electrolyte so self-charge caused by charge redistribution can be reduced.[4] Despite the research progress in suppressing self-discharge of SSSCs, further improvement is still necessary to reduce the OCV decay rates and leakage currents of SSSCs so they can be used as efficient energy storage devices. This is especially important for SSSCs to store energy collected by environmental energy harvesting devices such as piezoelectric or triboelectric nanogenerators due to the small and intermittent power delivered by these devices.[2,8]

Recently, super-concentrated salt solutions have been considered as electrolytes for supercapacitors (SCs) with expanded electrochemical stability window and reduced self-discharge.[15-17] However, in typical gel electrolytes for SSSCs, the concentrations of salts are in the range of 0.5 to 4 M.[4,12,14,18,19] Gel electrolytes with super-concentrated salt content larger than 10 M for SCs have been rarely reported.[20] This may be because most reported gel electrolytes for SCs are based on polymers such as polyvinyl alcohol (PVA), which are usually prepared via dissolution followed by coagulation in the electrolyte solutions.[10-12,18,22-25] But in super-concentrated salt solutions, these polymers cannot be dissolved well. In this work, we developed a polyacrylamide (PAAm) hydrogel loaded with LiCl solutions of high concentration as electrolytes for SSSCs. PAAm hydrogel is a superabsorbent polymer due to the difference in the osmotic pressure caused by the ionic groups inside and outside the hydrogel network.[20] We found super-

a. Beijing Institute of Nanoenergy and Nanosystems, Chinese Academy of Sciences, Beijing 101400, P. R. China.
b. School of Nanoscience and Technology, University of Chinese Academy of Sciences, Beijing 100049, P. R. China.
c. School of Materials Science and Engineering, Georgia Institute of Technology, Atlanta, GA 30332-0245, USA.
* Emails: zhong.wang@mse.gatech.edu, luxianmao@binn.cas.cn

concentrated LiCl solutions (up to 14 M) can be easily absorbed by PAAm hydrogel. Using PAAm hydrogel loaded with 14 M LiCl solution as the electrolyte of SCs, we showed that the self-discharge of the resulting SSSCs was significantly suppressed. Particularly, when the SSSCs were charged to 0.8 V, the OCV of the SSSCs dropped only 0.1 V in 24 hrs, and a low leakage current of 0.003 $\mu A\ mF^{-1}\ V^{-1}$ was also achieved. To the best of our knowledge, both the OCV decay rate and leakage current of our SSSCs with 14 M LiCl-PAAm hydrogel electrolyte are among the smallest reported for SCs with hydrogel electrolytes.[3,4,9-12,14,18,21-27] We further employed a triboelectric nanonenergator (TENG) to charge our SSSCs with 14 M LiCl-PAAm hydrogel electrolyte and demonstrated much improved charging efficiency due to the slow self-discharge.

Experimental

Chemicals and materials

Activated carbon (AC) (YEC-8A) was purchased from Yihuan Carbon Co. Ltd. (Fuzhou, China). Lithium chloride (LiCl, 99%), acrylamide (AAm, 99%), n,n'-methylenebisacrylamide (MBAAm, 99%), ammonium persulphate (APS, 99%), n,n,n',n'-tetramethylethylenediamine (TMED, 99%), n-methyl pyrrolidone (NMP, 99.9%) were purchased from Aladdin Reagent Co., Ltd. (Shanghai, China). Poly (vinylidene fluoride) (PVDF), acetylene black, and titanium and platinum plates were obtained from Lige Technology Co. Ltd. (Guangzhou, China). All chemicals and solvents were used as received without further purification. All aqueous solutions were prepared with ultrapure deionized water.

Preparation of hydrogel electrolytes

PAAm hydrogel electrolytes were prepared based on a method reported previously.[30] First, AAm monomer powder was dissolved in deionized water to form a 2.17 M solution. Next, MBAAm (0.06 wt.%) as the cross-linker and APS (0.16 wt.%) as the initiator were added to the AAm solution. After sonicating and degassing, the mixture was added with TMED (0.25 wt.%) as the accelerator. All weight percentages are relative to the mass of AAm monomer. The solution was then poured into a poly(methyl methacrylate) (PMMA) mold with dimensions of 2 × 2 × 0.2 cm. After 1 hr, the resulting gel was peeled off and dried in an oven at 80 °C for 24 hrs. Before the gel was used as electrolyte, it was soaked in an aqueous solution of 1 or 14 M LiCl (denoted as 1 or 14 M LiCl-PAAm) for a week.

Preparation of solid-state supercapacitors

AC, acetylene black, and PVDF binder were mixed in a mass ratio of 80:10:10 and dispersed in NMP to form a uniform slurry, which was then coated onto a Ti substrate (1 × 1 cm) as an electrode and dried under vacuum at 120 °C overnight. The mass loading of AC on each electrode was 1.5 mg cm^{-2}. To assemble symmetric solid-state supercapacitors, two electrodes were respectively pressed on the two sides of a piece of LiCl-PAAm hydrogel. Due to the strong adhesion of the hydrogel, the electrodes can be firmly attached to the hydrogel electrolyte.

Measurements

Scanning electron microscopy (SEM) was performed on a Nova NanoSEM 450. Cyclic voltammetry (CV) and galvanostatic charge-discharge (GCD) measurements were conducted on a Solartron 1287A potentiostat and a CHI 660E electrochemical workstation. Electrochemical impedance spectroscopy (EIS) measurements were carried out on a Solartron 1260A impedance analyzer over a frequency range from 10^6 to 0.1 Hz with an AC amplitude of 10.0 mV. Cycling stability tests were acquired by a LAND CT2001A battery test system. Self-discharge experiments were performed using an Arbin BT2000 battery testing system.

Before self-discharge measurement, the symmetric two-electrode cells were cycled for 50 times from 0 V to the desired voltages (0.8 V or 1.8 V) at a scan rate of 50 mV s^{-1}. Then the SCs were charged and discharged at 0.2 A g^{-1} between 0 V and the desired voltages for 20 cycles. Afterwards, the cells were charged at 0.2 A g^{-1} to the desired voltages and held for 2 hrs, during which the current responses (leakage currents) were recorded. Subsequently, the applied voltages were removed and the open circuit voltages (OCVs) of the cells were recorded. For the electrical output measurement of rotating triboelectric nanogenerator (R-TENG), a Keithley 6514 electrometer was used. The R-TENG consists of two stator and a rotator nonstructured based on reported methods[31] and it was connected to the supercapacitors via a rectifier. Charge/self-discharge curves of the supercapacitors were obtained on a CHI660D electrochemical workstation when the R-TENG was rotating at 500 rpm.

Results and discussion
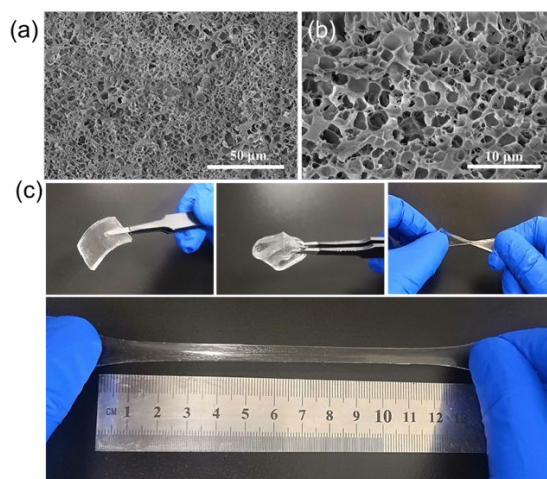
Fig. 1 (a, b) SEM images of freeze-dried PAAm hydrogel. (c) Digital graphs of a piece of PAAm hydrogel showing its good mechanical property.

SEM images of the freeze-dried PAAm hydrogel reveal a three-dimensional (3D) porous structure with an average pore size of 1.5 μm (Fig. 1a, b). This porous network structure is favorable for electrolyte absorption and diffusion. In addition, the PAAm hydrogel exhibited high flexibility and stretchability. It can be easily twisted and stretched up to 1300% in length (Fig. 1c),

indicating the PAAm hydrogel is suitable for integrating with flexible or wearable electronic devices.
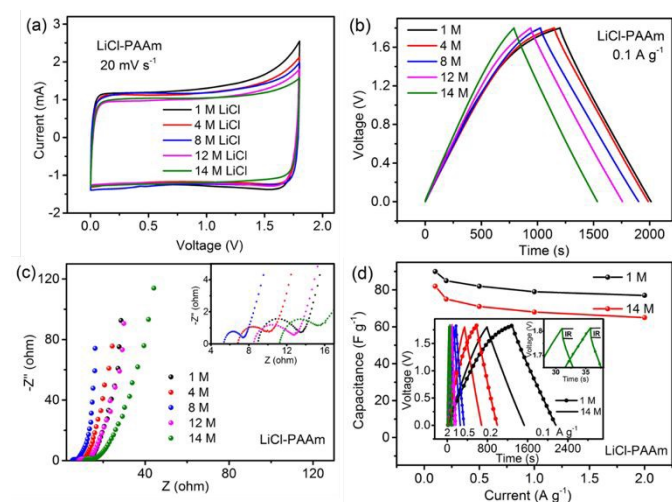

Fig. 2 (a) CV curves at a scan rate of 20 mV s^{-1}, (b) GCD curves at 0.1 A g^{-1}, (c) EIS, and (d) rate performances of SSSCs using 1 and 14 M LiCl-PAAm hydrogel electrolytes. Insets are the corresponding GCD curves at different current densities and IR drops due to the ESRs of the SSSCs when discharged at 2 A g^{-1}.

Fig. 2 shows the electrochemical performances of the SSSCs with PAAm hydrogel soaked with 1, 4, 8, 12 and 14 M LiCl electrolytes. CV curves exhibited a quasi-rectangle shape, indicating good capacitive behavior of the SSSCs (Fig. 2a). GCD curves at 0.1 A g^{-1} of the SSSCs are shown in Fig. 2b. Based on discharging times, the specific capacitances were estimated to be 90, 93, 97, 91 and 82 F g^{-1} for 1, 4, 8, 12 and 14 M LiCl-PAAm hydrogel electrolytes, respectively. The highest specific capacitance was obtained from 8 M LiCl-PAAm electrolyte, which may be attributed to its higher ionic conductivity than the electrolytes of other concentrations.[32] Fig. 2c shows that the Nyquist plot of each SSSC consists of an incomplete semicircle at the high frequency region and a straight line at the low frequency region, with an equivalent series resistance (ESR) in the range of 5-11 ohm. Rate performances of the SSSCs using 1 and 14 M LiCl-PAAm electrolytes at various charging current densities are shown in Fig. 2d. When the current densities were increased from 0.1 to 2 A g^{-1}, 86% and 80% of the specific capacitances for the SSSCs with 1 and 14 M LiCl-PAAm electrolytes were retained. In addition, when discharged at large currents, the SSSCs showed voltage drops (IR) caused by ESR. For SSSCs using 1 and 14 M LiCl-PAAm electrolytes, the IRs were 37 and 44 mV at 2 A g^{-1} (Fig. 2d, inset), respectively, consistent with the ESRs obtained from EIS measurements (Fig. 2c, inset).

The self-discharge rates of the SCs were first evaluated based on their open circuit voltages (OCVs). Figs. 3a and 3c show decreased OCVs of the cells after they were charged at 0.2 A g^{-1} to 0.8 or 1.8 V followed by 2-hr float charging. With a charging voltage of 0.8 V, the OCVs dropped to 0.17, 0.29, 0.47, 0.62 and 0.70 V after 24 hrs for the SSSCs using 1, 4, 8, 12 and 14 M LiCl-PAAm hydrogel electrolytes, respectively (Fig. 3a). When the same SSSCs were charged to 1.8 V, their OCVs dropped to 0.38, 0.54, 0.78, 1.15 and 1.40 V after 24 hrs, respectively (Fig. 3c).

Clearly, the self-discharge rate of the cells decreased with the increase of LiCl concentration in the gel electrolytes. The leakage currents at 0.8 and 1.8 V are shown in Figs. 3b and 3d. For the SSSCs with 1, 4, 8, 12 and 14 M LiCl-PAAm, their respective leakage currents stabilized at 8.7, 5.0, 2.5, 1.7 and 0.15 µA at 0.8 V, while increased leakage currents of 25.5, 16.5, 10.0, 5.6 and 2.4 µA were observed for the SSSCs charged at 1.8 V. For both charging voltages, the leakage currents decreased substantially with the increase of electrolyte concentration. The much smaller leakage currents at higher electrolyte concentrations further confirmed the reduced self-discharge at higher concentrations. It is worth noting that both the OCV decay rate (0.1 V in 24 h) and the leakage current (0.003 µA mF^{-1} V^{-1} at 0.8 V) of the SSSC using 14 M LiCl-PAAm hydrogel electrolytes are among the smallest reported in the literature (Table 1).[3,4,9-12,14,18,21-27] As shown in Fig. 3e, similar OCV decay rates were observed for the SSSC under flat and bending states, indicating that bending did not affect much of the self-discharge rate. This may be attributed to the good adhesion between PAAm gel and the Ti substrate. It should be noted that the charging current can affect the OCV decay rate if the SCs were charged without float charging due to charge redistribution. As shown in Fig. 3f, for the SSSC with 14 M LiCl-PAAm hydrogel electrolyte charged to 1.80 V at current densities of 0.02, 0.2, 1 and 5 A g^{-1}, the OCV dropped to 1.36, 1.30, 1.18 and 0.93 V after 24 hrs, respectively. However, by adding a float charging stage after the SSSCs were charged at constant current, the OCV decay rates became unaffected by the charging current densities (Fig. 3g-h). This result indicates that if the effect of charge redistribution is eliminated, the self-discharge rate should be consistent under different charging currents.

To further understand the self-discharge mechanism of the SSSCs, we monitored the open circuit potentials (OCPs) of both positive and negative electrodes of charged cells using a silver wire as the reference electrode. As shown in Fig. 4, the decreasing OCPs of the positive electrodes and increasing OCPs of the negative electrodes indicate that both electrodes suffered from self-discharge. Consistent with the overall OCV drop, the potential drop of the positive electrodes and the potential increase of the negative electrodes decreased with the increase of the electrolyte concentration, indicating suppressed self-discharge at higher salt concentration.

Self-discharge of supercapacitors can be attributed to three pathways: 1) charge redistribution in the pores of the electrodes; 2) internal ohmic leakage; 3) faradaic reactions with activation- or diffusion-controlled mechanism.[5,33,34-39] Based on the large leakage resistances of the SSSCs (~10^7 ohm) estimated from the EIS results in Fig. 2c, the ohmic leakage should be small. Also, since we added 2-hr float charging before OCP decay tests, the contribution from charge redistribution can be excluded. Therefore, the potential decays can be simulated based on faradaic reaction mechanisms using the following formula $V_t = f(t)$:[3,33]

$$V_t = V_i - mt^{1/2} - a - bln\left(t + \frac{CK}{i_0}\right)$$

Where V_t is the electrode potential at discharge time t, V_i is the initial potential of the charged electrode, C is the capacitance, T

ARTICLE

is the absolute temperature, i_0 is the exchange current density, m is a constant related to the diffusion coefficient of the redox species, F is Faraday constant, K is an integration constant, and a, b are constants related to the faradaic process which can be expressed as follows:

$$a = \frac{RT}{\alpha F}\ln\left(\frac{\alpha F i_0}{RTC}\right); \quad b = \frac{RT}{\alpha F}$$

where α is charge transfer coefficient.
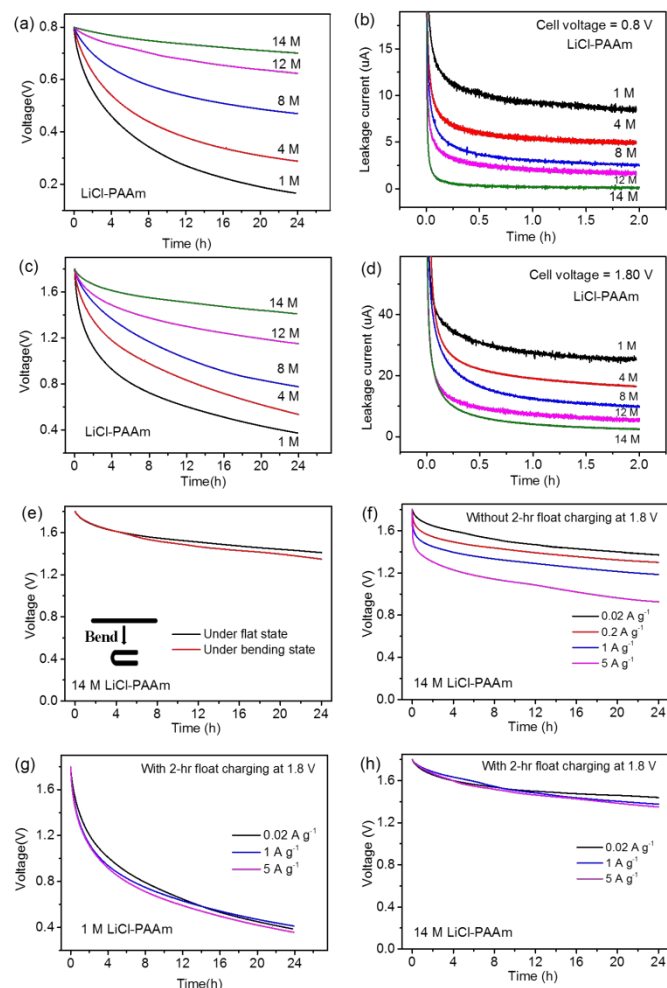
Fig. 3 (a) OCV decays and (b) leakage currents for SSSCs using LiCl-PAAm hydrogel electrolytes with a charging voltage of 0.8 V. (c) OCV decays and (d) leakage currents for

the SSSCs with a charging voltage of 1.8 V. (e) OCV decays of the SSSC used 14 M LiCl-PAAm hydrogel electrolyte under flat and bending states. (f,g,h) OCV decays of SSSCs charged to 1.8 V at different current densities: (f) 14 M LiCl-PAAm, without float charging, (g) 1 M LiCl-PAAm hydrogel electrolyte, with 2-h float charging, (h) 14 M LiCl-PAAm, with 2-h float charging.

Based on the above equation, the potential profiles of the positive and negative electrodes using 1 and 14 M LiCl-PAAm electrolytes were fitted with parameters listed in Table 2. It is clear that the simulated and measured potential changes match well. For the cell with 1 LiCl-PAAm hydrogel electrolytes at a charging voltage of 0.8 V, the potential changes for both positive and negative electrodes fit well with activation-controlled faradaic model (Fig. 4a). While for 14 M LiCl-PAAm hydrogel electrolyte at 0.8 V, the simulated potential changes match closely with the diffusion-controlled faradaic model (Fig. 4b). For 1 M LiCl-PAAm SCs charged to a high voltage of 1.8 V, activation-controlled faradaic process still dominated the self-discharge of both positive and negative electrodes (Fig. 4c); while for 14 M LiCl-PAAm hydrogel electrolyte, the self-charge was caused by mixed activation- and diffusion-controlled faradaic processes (Fig. 4d).
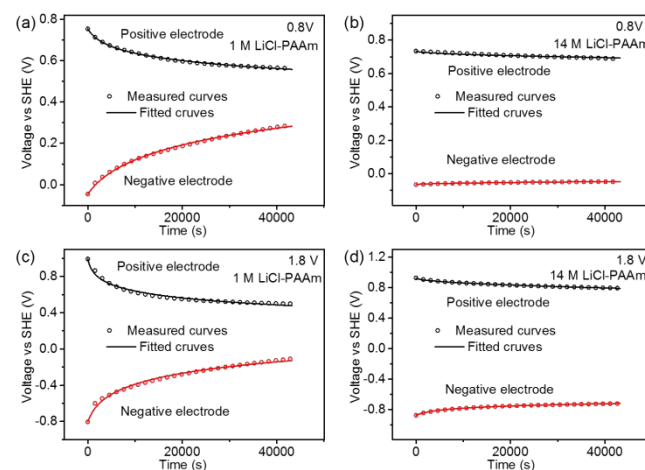

Fig. 4 OCP profiles and fitted curves of the positive and negative electrodes for SSSCs with (a) 1 M LiCl-PAAm, charged to 0.8 V, (b) 14 M LiCl-PAAm, charged to 0.8 V, (c) 1 M LiCl-PAAm, charged to 1.8 V, and (d) 14 M LiCl-PAAm, charged to 1.8 V. Dotted and solid curves represent the measured and fitted results, respectively.

Table 1. Comparison of self-discharge rates for supercapacitors using hydrogel electrolytes.

Electrode	Hydrogel electrolyte	OCV decay rate	Leakage current	Ref
AC fiber cloth	PAAK/KOH	0.8→0.2 V (40 h)	0.16 mA cm^{-2}	21
AC fiber cloth	PVA/GA /H$_2$SO$_4$	0.8→0.2 V (20 h)	0.08 mA cm^{-2}	9
PANI/CNT film	PVA/H$_2$SO$_4$	0.8→0.5 V (4 h)	17.2 µA	22
AC	PVA/KOH/KI	0.8→0.3 V (10 h)		23
CNPs/MnO$_2$	PVA/H$_3$PO$_4$	0.8→0.2 V (24 h)	10 µA	18
GHs	PVA/H$_2$SO$_4$	0.8→0.5 V (4 h)	0.019 µA mF^{-1} V^{-1}	10
GHs	PVA/H$_2$SO$_4$	0.8→0.4 V (24 h)	0.03 µA mF^{-1} V^{-1}	24
Graphene paper	PVA/H$_3$PO$_4$	1→0.6 V (2.5 h)	13 µA	11
Graphene/PANI	PVA/H$_2$SO$_4$	0.8→0.53 V (4 h)	0.015 µA mF^{-1} V^{-1}	25
Porous carbon cloth	PVA/CuCl$_2$/H$_2$SO$_4$	0.8→0.4 V (5 h)		12
		0.8→0.2 V (22 h)		
Ti$_3$C$_2$T$_X$ MXene	PVA/H$_3$PO$_4$	0.6→0.4 V (2 h)		26
Graphene film	PPDP/LiCl	0.8→0.4 V (12 h)	0.15 µA mF^{-1} V^{-1}	3
AC	PVA/Li$_2$SO$_4$/CNT/ BMIMBr	1.8→1.18 V (5 h)		14
AC fabric	Agar/K$_2$SO$_4$	1.8→1 V (12 h)		27
CNTs	NaPSS/PVA/H$_3$PO$_4$ /PDDACl	0.8→0.4 V (8 h)		4
CNTs/PANI	NaPSS/PVA/H$_3$PO$_4$ /PDDACl	0.8→0.4 V (20 h)		4
AC	**PAAm/14 M LiCl**	**0.8→0.7 V (24h)**	**0.003 µA mF^{-1} V^{-1}**	**This work**
		1.8→1.4 V (24 h)	**0.022 µA mF^{-1} V^{-1}**	

Abbreviations: PAAK: potassium poly (acrylate); PVA: polyvinyl alcohol; GA: glutaraldehyde; PANI: polyaniline; CNTs: carbon nanotubes; CNPs/MnO$_2$: carbon nanoparticles/MnO$_2$ nanorods hybrid structure; GHs: Graphene hydrogels; PPDP: poly (propylsulfonate dimethylammonium pro-pylmethacrylamide); BMIMBr: 1-butyl-3-methylimidazolium bromide; NaPSS: sodium polystyrene sulfonate; PDDACl: poly(diallyl dimethylammonium chloride).

Table 2. Fitting parameters for the OCP decays of positive and negative electrodes.

Concentration	Cell voltage	Electrode	m (V s$^{-1/2}$)	a (V)	b
1 M	0.8 V	Positive		-0.42	0.058
1 M	0.8 V	Negative		-1.121	0.135
1 M	1.8 V	Positive		-0.687	0.113
1 M	1.8 V	Negative		-1.363	0.191
14 M	0.8 V	Positive	0.00018		
14 M	0.8 V	Negative	0.00009		
14 M	1.8 V	Positive	0.00065		
14 M	1.8 V	Negative		-0.341	0.046

The above simulation results suggest that the self-discharge mechanism transited from an activation-controlled to diffusion-controlled faradaic process when the gel electrolytes were switched from 1 M to 14 M LiCl-PAAm. This change maybe explained with the decreased activation-controlled faradaic side reactions involving water in the LiCl-PAAm hydrogel electrolytes at higher concentration.[40-48] With aqueous electrolytes, side reactions such as oxidation/reduction of the functional groups on the surface of activated carbon, corrosion of carbon, and water oxidation/reduction in the electrolyte may occur.[41] For examples,

corrosion of carbon:
$$H_2O - ne^- \rightarrow OH^{\cdot} + H^+ \ (n=1), O^{\cdot} + 2H^+ \ (n=2)$$
$$C + O^{\cdot}/OH^{\cdot} \rightarrow C = O, C - OH_{ads} \rightarrow CO(+H^+)$$
$$C + 2H_2O - 4e^- \rightarrow CO/CO_2\uparrow + 4H^+$$

evolution of O$_2$:
$$2H_2O - 4e^- \rightarrow O_2 + 4H^+$$
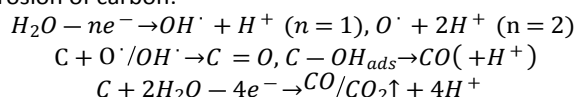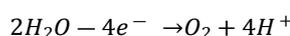
evolution of H$_2$:
$$\langle CH_x \rangle + yH_2O + ye^- \rightarrow yH_2 + yOH^- + C$$
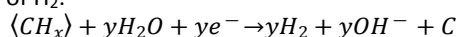
The above reactions would consume the electrode charges and cause self-discharge. Notably, many of the side reactions involve free water molecules. Using highly concentrated electrolyte, the water molecules are largely bond to Li$^+$ ions, leading to decreased activity of water molecules.[3,49,50] As a result, these side reactions involving free water molecules near the electrode surface become more sluggish, leading to slow self-discharge rate and shift of the self-discharge process from activation-controlled to diffusion-controlled faradaic mechanism. It should be noted that the increased electrolyte concentration may also impede electron transfer between redox molecules and electrode surface. Wang et al. have found that both electron and ion transfers take place at the liquid-solid interface when an electrode is in contact with electrolyte.[51,52] For charged supercapacitors, due to the high mobility and thermal instability of electrons, a large discharging rate may occur at interface. In addition, electron transfer can also be impeded because of the change of dielectric environment around the redox species at high electrolyte

concentrations, leading to slow self-discharge caused by faradaic processes. [53,54]

Self-discharge of supercapacitors has an extremely negative effect on their capacity for energy storage, especially when they are used for storing energy collected by environmental energy harvesting devices that deliver small power at μW/mW scales. [33] If the electric current delivered by the energy harvesting devices is less than the leakage current of the supercapacitors, they cannot be charged to the desired voltage for powering electronic devices. Reduction of the leakage current for supercapacitors should enhance energy storage efficiency and reduce charging time. To demonstrate this point, we employed a triboelectric nanogenerator (TENG) to charge the SSSCs with PAAm gel electrolytes (Fig. 5a). The TENG was a low-friction rotating TENG (R-TENG) consisting of two stators and a rotor. Details of the R-TENG can be found in previous report. [31] When the rotor was rotating at 500 rpm, the measured open circuit voltage and peak short circuit current of the R-TENG were approximately 350 V and 8.5 μA, respectively (Fig. 5b, c). Fig. 5d shows the charging/discharging process powered by the R-TENG and the decay of OCVs after the SSSCs were charged. It should be noted that due to the small current delivered the R-TENG, the capacitances of the SSSCs used for charging were 6 mF. For the SSSC with 1 M LiCl-PAAm hydrogel electrolyte, it took nearly an hour (3545 s) to charge to 0.82 V. The SSSC cannot be charged to a higher voltage due to increased leakage current that became larger than the current delivered by the R-TENG. While for the SSSC using 14 M LiCl-PAAm hydrogel electrolyte, it only took 678 sec to charge to 0.82V, much shorter than the SSSC with 1 M LiCl-PAAm electrolyte. Also, the SSSC using 14 M LiCl-PAAm hydrogel electrolyte can be easily charged to 1.8 V after 2457 s. The much faster and more efficient charging process of the SSSC with 14 M LiCl-PAAm hydrogel electrolyte benefits considerably from its smaller leakage current. When discharged at a constant current of 0.1 A g^{-1} after TENG charging, the SSSCs with 1 and 14 M PAAm-LiCl hydrogel electrolytes delivered specific capacitances of 94 and 86 F g^{-1}, respectively, close to the capacitances obtained from their GCDs in Fig. 2b. Furthermore, after TENG charging, the SSSC with 14 M PAAm-LiCl electrolyte exhibited slower self-discharge compared to the one with 1 M PAAm-LiCl electrolyte (Fig. 5d). This result demonstrates the potential of combining our SSSCs using LiCl-PAAm hydrogel electrolyte with energy harvesting devices to form efficient self-powered units as energy supply for portable electronic devices.
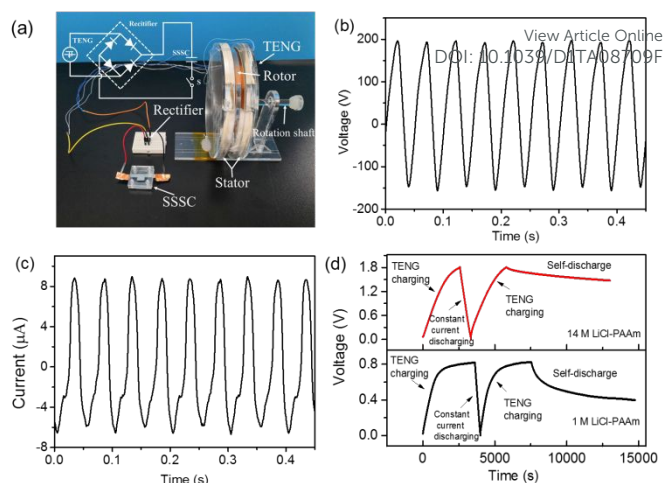

Fig. 5 (a) Circuit for charging SSSC by R-TENG. Inset shows the circuit diagram. (b, c) Open circuit voltage and short circuit current provided by the R-TENG. (d) TENG charging/constant-current discharging and TENG charging/OCV decays of SSSCs with 1 and 14 M PAAm-LiCl hydrogel electrolytes.

Conclusions

In summary, we have prepared a PAAm hydrogel that can be loaded with highly concentrated LiCl electrolytes for SSSCs. With the increase in concentration of LiCl-PAAm electrolytes, the self-discharge rate of the resulting SSSCs decreased substantially. This can be attributed to the reduction of the activity of free water molecules in highly concentrated LiCl-PAAm hydrogel electrolytes that led to a shift of the self-discharge process from activation-controlled to diffusion-controlled faradaic mechanism. For SSSCs with 14 M LiCl-PAAm hydrogel electrolyte, a low OCV decay rate (6.7×10^{-5} V mF^{-1} hr^{-1}) and a small leakage current (0.003 μA mF^{-1} V^{-1}) at 0.8 V were obtained. Owing to the significantly suppressed self-discharge, which is among the slowest reported self-discharge rates of SSSCs using hydrogel electrolytes, our SSSCs allowed much improved charging efficiency for storing energy collected by a triboelectric nanogenerator, demonstrating their potential to be combined with environmental energy harvesters as self-powered energy units to drive flexible or wearable devices.

Author Contributions

M.S., Z.L.W. and X.L. planned the study. M.S. fabricated supercapacitor cells and conducted electrochemical testing and material characterizations. M.S., W.Y., Z.Z., M.Z. and X.L. performed data analysis. Z.L.W. and X.L. supervised the study. All authors have given approval to the final version of the manuscript.

Conflicts of interest

There are no conflicts to declare.

Acknowledgements

References

1   Z. Wang, H. Li, Z. Tang, Z. Liu, Z. Ruan, L. Ma, Q. Yang, D. Wang and C. Zhi, *Adv. Funct. Mater.*, 2018, **23**, 1804560.
2   K. Liu, C. Yu, W. Guo, L. Ni, J. Yu, Y. Xie, Z. Wang, Y. Ren and J. Qiu, *J. Energy Chem.*, 2021, **58**, 94-109.
3   K. Ge and G. Liu, *Chem. Commun.*, 2019, **55**, 7167-7170.
4   X. Wang, Y. Liu, H. Li, X. Wang, Y. Liu, H. Li, T. Lv, J. Wan, K. Dong, Z. Chen and T. Chen, *Small*, 2021, **17**, 2102054.
5   H. A. Andreas, *J. Electrochem. Soc.*, 2015, **162**, A5047-A5053.
6   I. S. Ike, I. Sigalas and S. Iyuke, *J. Electron. Mater.*, 2018, **47**, 470-492.
7   A. Lewandowski, P. Jakobczyk, M. Galinski and M. Biegun, *Phys. Chem. Chem. Phys.*, 2013, **15**, 8692-8698.
8   M. Zhao, J. Nie, H. Li, M. Xia, M. Liu, Z. Zhang, X. Liang, R. Qi, *Nano Energy*, 2019, **55**, 447-453.
9   H. Wada, K. Yoshikawa, S. Nohara, N. Furukawa, H. Inoue, N. Sugoh, H. Iwasaki and C. Iwakura, *J. Power Sources,* 2006, **159**, 1464-1467.
10 Y. Xu, Z. Lin, X. Huang, Y. Wang, Y. Huang and X. Duan, *Advanced Materials*, 2013, **25**, 5828-5828.
11 J. Zang, C. Cao, Y. Feng, J. Liu and X. Zhao, *Sci. Rep.*, 2014, **4**, 6492.
12 H. Wang, J. Chen, R. Fan and Y. Wang, *Sustain. Energy Fuels*, 2018, **2**, 2727-2732.
13 M. L. Verma, M. Minakshi and N. K. Singh, *Electrochim. Acta*, 2014, **137**, 497-503.
14 L-Q. Fan, Q-M. Tu, C-L. Geng, J-L. Huang, Y. Gu, J-M. Lin, Y-F. Huang and J-H. Wu, *Electrochim. Acta*, 2019, **331**, 135425.
15 D. Xiao, Q. Wu, X. Liu, Q. Dou, L. Liu, B. Yang and H. Yu, *ChemElectroChem*, 2019, **6**, 439-443.
16 Z. Tian, W. Deng, X. Wang, C. Liu, C. Li, J. Chen and F. Pan, *Funct. Mater. Lett.*, 2017, **10**, 1750081.
17 P. Galek, E. Frackowiak and K. Fic, *Electrochim. Acta*, 2019, **334**, 135572.
18 L. Yuan, X. Lu, X. Xiao, T. Zhai, J. Dai, F. Zhang, B. Hu, X. Wang, L. Gong, J. Chen, C. Hu, Y. Tong, J. Zhou and Z. L. Wang, *ACS Nano*, 2012, **6**, 656.
19 H. Li, T. Lv, N. Li, Y. Yao, K. Liu and T. Chen, *Nanoscale*, 2017, **9**, 18474-18481.
20 H. Wang, J. Liu, J. Wang, M. Hu, Y. Feng, P. Wang and Q. Yuan, *ACS Appl. Mater Inter.*, 2018, **11**, 49-55.
21 S. Nohara, H. Wada, N. Furukawa, H. Inoue and C. Iwakura, *Res. Chem. Intermediat.*, 2006, **32**, 491-496.
22 C. Meng, C. Liu, L. Chen, C. Hu and S. Fan, *Nano Lett.*, 2010, **10**, 4025-4031.
23 H. Yu, J. Wu, L. Fan, K. Xu, X. Zhong, Y. Lin and J. Lin, *Electrochim. Acta*, 2011, **56**, 6881-6886.
24 Y. Xu, Z. Lin, X. Huang, Y. Liu, Y. Huang and X. Duan, *ACS Nano*, 2013, **7**, 4042-4049
25 K. Li, J. Liu, Y. Huang, F. Bu and Y, Xu, *J. Mater. Chem. A*, 2017, **5**, 5466-5474.
26 Q. Jiang, C. Wu, Z. Wang, A. Chi. Wang, J-H. He, Z. L. Wang and H. N. Alshareef, *Nano Energy*, 2018, **45**, 266–272
27 J. Menzel, E. Frckowiak and K. Fic, *Electrochim. Acta*, 2020, **332**, 135435.
28 L. Petit, R. Vuilleumier, P. Maldivi and C. Adamo, *J. Chem. Theory Comput.*, 2008, **4**, 1040-1048.
29 L. Suo, O. Borodin, T. Gao, M. Olguin, J. Ho, X. Fan and K. Xu, *Science*, 2015, **350**, 938-943.
30 C. C. Kim, H. H. Lee, K. H. Oh and J. Y. Sun. *Science*, 2016, **353**, 682-687.
31 P. Chen, J. An, S. Shu, R. Cheng, J. Nie, T. Jiang and Z. L. Wang, *Adv. Energy Mater.*, 2021, **11**, 2003066.
32 K Tanaka, R Tamamushi. Zeitschrift für Naturforschung A, 2014, **46**, 141-147.
33 M. Xia, J. Nie, Z. Zhang, X. Lu and Z. L. Wang, *Nano Energy*, 2018, **47**, 43-50.
34 J. Niu, B. E. Conway and W. G. Pell, *J. Power Sources*, 2004, **135**, 332-343.
35 H. A. Andreas, J. M. Black and A. A. Oickle, *Electrochim. Acta*, 2014, **140**, 116-124.
36 B. E. Conway, W. G. Pell and T. C. Liu, *J. Power Sources*, 1997, **65**, 53-59.
37 H. Yang and Y. Zhang, *J. Power Sources*, 2011, **196**, 8866-8873.
38 M. Kaus, J. Kowal and D. U. Sauer, *Electrochim. Acta*, 2010, **55**, 7516-7523.
39 Y. Diab, P. Venet, H. Gualous, G. Rojat, *IEEE Trans. Power Electron.*, 2009, **24**, 510-517.
40 L. García-Cruz, P. Ratajczak, J. Iniesta, V. Montiel and F. Béguin, *Electrochim. Acta*, 2016, **202**, 66-72.
41 M. He, K. Fic, E. Fra, P. Novák and E. J. Berg, *Energy Environ. Sci.*, 2016, **9**, 623-633.
42 A. M. Oickle, J. Tom and H. A. Andreas, *Carbon*, 2016, **110**, 232-242.
43 Y. Xie, W. Qiao, W. Zhang, G. Sun and L. Ling, *New Carbon Mater.*, 2010, **25**, 248-254.
44 B. Avasarala, R. Moore, P. Haldar, *Electrochim. Acta*, 2010, **55**, 4765-4771.
45 K. Jurewicz, E. Frackowiak and F. Béguin, *Appl. Phy. A*, 2004, **78**, 981-987.
46 P. Ratajczak, K. Jurewicz and F. BÚguin, *J. Appl. Electrochem.*, 2014, **44**, 475-480.
47 Q. Gao, L. Demarconnay, E. Raymundo-Piñero and F. Béguin, *Energy Environ. Sci.*, 2012, **5**, 9611-9617.
48 F. Béguin, K. Kierzek, M. Friebe, A. Jankowska, J. Machnikowski, K. Jurewicz and E. Frackowiak, *Electrochim. Acta*, 2006, **51**, 2161-2167.
49 M. B. Singh, V. H. Dalvi and V. G. Gaikar, *RSC Adv.*, 2015, **5**, 15328-15337.
50 J. Zheng, G. Tan, P. Shan, T. Liu, J. Hu, Y. Feng, L. Yang, M. Zhang, Z. Chen, Y. Lin, J. Lu, J. C. Neuefeind, Y. Ren, K. Amine, L-W. Wang, K. Xu and F. Pan, *Chem*, 2018, **4**, 2872-2882.
51 S. Lin, L. Xu, A. C. Wang and Z. L. Wang, *Nat. Commun.* 2020, **11**,399.
52 S. Lin, X. Chen and Z. L. Wang, *Chem. Rev.* 2021, doi:10.1021/acs.chemrev.1c00176.
53 G. Das, S. Hlushak, M. C. Ramos and C. McCabe, AIChE J. 2015, **61**, 3053-3072.
54 A. P. Abbott and J. F. Rusling, J. Phys. Chem. 1990, **94**, 8910-8912.